Effects of number of parallel runs and frequency of bias-strength replacement in generalized ensemble molecular dynamics simulations

Takuya Shimato [Equal first author, 1], **Kota Kasahara** [Corresp., Equal first author, 2], **Junichi Higo** [3], **Takuya Takahashi** [2]

[1] Graduate School of Life Sciences, Ritsumeikan University, Kusatsu, Shiga, Japan

[2] College of Life Sciences, Ritsumeikan University, Kusatsu, Shiga, Japan

[3] Graduate School of Simulation Studies, University of Hyogo, Kobe, Hyogo, Japan

Corresponding Author: Kota Kasahara
Email address: ktkshr@fc.ritsumei.ac.jp

Background. The generalized ensemble approach with the molecular dynamics (MD) method has been widely utilized. This approach usually has two features. (i) A bias potential, whose strength is replaced during a simulation, is applied. (ii) Sampling can be performed by many parallel runs of simulations. Although the frequency of the bias-strength replacement and the number of parallel runs can be adjusted, the effects of these settings on the resultant ensemble remain unclear.

Method. In this study, we performed multicanonical MD simulations for a foldable mini-protein (Trp-cage) and two unstructured peptides (8- and 20-residue poly-glutamic acids) with various settings.

Results. As a result, running many short simulations yielded robust results for the Trp-cage model. Regarding the frequency of the bias-potential replacement, although using a high frequency enhanced the traversals in the potential energy space, it did not promote conformational changes in all the systems.

Effects of number of Parallel Runs and Frequency of Bias-Strength Replacement in Generalized Ensemble Molecular Dynamics Simulations.

Takuya Shimato,[1,†] Kota Kasahara,[2,†,*] Junichi Higo[3], and Takuya Takahashi[2]

Graduate School of Life Sciences, Ritsumeikan University, Kusatsu, Shiga, Japan
College of Life Sciences, Ritsumeikan University, Kusatsu, Shiga, Japan
Graduate School of Simulation Studies, University of Hyogo, Kobe, Hyogo, Japan
† The first two authors are considered to be joint first authors.

Corresponding Author:
Kota Kasahara
Graduate School of Life Sciences, Ritsumeikan University, 1-1-1 Noji-higashi, Kusatsu, Shiga, Japan 525-8577
Email address: ktkshr@fc.ritsumei.ac.jp

Abstract

Background. The generalized ensemble approach with the molecular dynamics (MD) method has been widely utilized. This approach usually has two features. (i) A bias potential, whose strength is replaced during a simulation, is applied. (ii) Sampling can be performed by many parallel runs of simulations. Although the frequency of the bias-strength replacement and the number of parallel runs can be adjusted, the effects of these settings on the resultant ensemble remain unclear.
Method. In this study, we performed multicanonical MD simulations for a foldable mini-protein (Trp-cage) and two unstructured peptides (8- and 20-residue poly-glutamic acids) with various settings.
Results. As a result, running many short simulations yielded robust results for the Trp-cage model. Regarding the frequency of the bias-potential replacement, although using a high frequency enhanced the traversals in the potential energy space, it did not promote conformational changes in all the systems.

Introduction

In the past several decades, the molecular dynamics (MD) method has been widely applied to investigate the microscopic behavior of molecular systems. Although advances in high-performance computing technology have extended the timescale that is reachable by MD

simulations (Salomon-Ferrer et al., 2013; Shaw et al., 2014; Abraham et al., 2015), there is still a large gap from experimental measurements. In particular, it is not straightforward to characterize the free-energy landscape (FEL) of a complex molecular system, because the characteristics of conformational ensembles obtained via canonical MD simulations largely depend on the initial conditions. To solve this problem, the generalized ensemble (GE) approach has been extensively developed and applied to the MD method. The GE approach enhances the conformational sampling using some tricks. First, in many GE methods, the conformational sampling can be performed with many parallel runs of simulations in a coupled or independent manner. For example, the replica-exchange MD (REMD) method (Sugita & Okamoto, 1999) involves performing many simulations of the same system, i.e., replicas, with different temperatures. The replicas with adjacent temperatures are coupled by exchanging their temperatures via Monte Carlo trials. On the other hand, the multicanonical MD (McMD) method (Nakajima, Nakamura & Kidera, 1997) can be performed by multiple independent runs, and a resultant ensemble is obtained by concatenating the trajectories of these runs (Ikebe et al., 2010). Second, the GE approach generates a non-Boltzmann distribution by applying bias potential, e.g., heating/cooling in the entire system or a part of the system, scaling the potential energies, and applying spring potentials for parts of system. These biases enhance the conformational changes of molecules and avoid trapping the molecular system at local minima in the FEL. During a simulation, the strength of the bias is frequently replaced, and the system alternates between different bias conditions. After simulations, a canonical ensemble can be obtained by reweighting each snapshot in the sampled conformational ensemble (Souaille & Roux, 2001; Shirts & Chodera, 2008).

For using these two features, users must adjust some settings. First, the number of runs is an adjustable parameter. In the case of the REMD method, using a larger number of replicas allows wider overlaps of the energy distributions between adjacent replicas and results in a higher acceptance probability. However, increasing the number of runs proportionally increases the computational costs. Users must choose the optimal balance between the number of runs and the length of each run according to the available computational resources. Previously, Ikebe et al. reported that an increase in the number of independent runs of McMD yields efficient exploration of a wider area of the conformational space. (Ikebe et al., 2010) However, the balance between the number of runs and the length of each run has not been discussed. Second, the frequency of the bias-strength replacement is also adjustable. In the REMD method, the frequency of replica-exchange trials must be specified by users. Other methods using a continuous bias strength, e.g., McMD and adaptive umbrella sampling (AUS), can control the frequency of bias-strength replacement by using the virtual-system coupling scheme, (Higo, Umezawa & Nakamura, 2013; Higo et al., 2015) as described later. It is reported that the frequency of the bias-strength replacement affects the resultant ensembles for the REMD method. Although higher frequencies enhance the traversals in the temperature space, they are suspected as an origin of artifacts. (Periole & Mark, 2007; Sindhikara, Meng & Roitberg, 2008; Rosta & Hummer, 2009; Sindhikara, Emerson & Roitberg, 2010; Jani, Sonavane & Joshi, 2014;

Iwai, Kasahara & Takahashi, 2018) Although the effects of these features have been examined, these studies were mainly based on simple model peptides with helix–coil transitions. The effects of the features for more practical cases, e.g., a protein folding–unfolding transition, are not fully understood. More importantly, the relationship between these effects and the complexities of molecular systems, e.g., the degree of freedom and ruggedness of the free-energy landscape, are expected to be revealed.

In this study, we aim to elucidate the effects of the number of runs and the bias-replacing frequency for the GE method on the resultant conformational ensembles of molecular models including a foldable mini-protein and disordered model peptides. We utilized the trivial-trajectory parallelized virtual-system coupled McMD (TTP-V-McMD) method (Ikebe et al., 2010; Higo, Umezawa & Nakamura, 2013), which is a variant of the McMD method, for simulating the three molecular models with an explicit solvent: (i) Trp-cage, (ii) 8-residue poly-glutamic acid (PGA8), and (iii) 20-residue poly-glutamic acid (PGA20). We chose these models as test cases to examine the simulation conditions because they are sufficiently small for elucidating their conformational ensembles within a practical computational time in addition to the fact that their structural properties have been well studied thus far. Trp-cage, which is a mini-protein consisting of 20 amino acids, has been widely studied as a prominent model of protein folding. (Ahmed et al., 2005; Péter Hudáky et al., 2007; Hałabis et al., 2012) Poly-glutamic acids have been used as model peptides to characterize the conformational properties of polypeptides. (Clarke et al., 1999; Kimura et al., 2002; Finke et al., 2007; Donten & Hamm, 2013; Ogasawara et al., 2018) We analyzed their FELs under various parameter settings to provide a guide for adjusting these parameters for the GE methods. The questions to be answered are as follows: “Which condition is more efficient: many short simulations or a small number of long-term simulations?” and “Which is better: frequent or less frequent replacement of the bias strength?”. Moreover, we discuss the relationship between the relaxation of the energy and that of the protein conformation. While the McMD method enhances the relaxation in the energy space, it is not guaranteed to enhance the relaxation in the conformational space. We analyzed these two relaxation processes using the McMD trajectories calculated with the various settings.

Materials & Methods

We calculated the FELs of the three explicitly solvated molecular models: Trp-cage, PGA8, and PGA20, by using the TTP-V-McMD method with various settings. The theory of McMD, virtual-system coupled McMD (V-McMD), and trivial-trajectory parallelization (TTP) is briefly presented in the following subsections. Then, the simulation protocol applied in this study is described.

McMD

The McMD method efficiently explores the conformational space of a molecular system, by applying a biasing energy term. The Hamiltonian H of the system is

$$H = K + E_{mc}, \quad (1)$$

where K and E_{mc} denote the kinetic energy and multicanonical energy, respectively. E_{mc} is defined as follows:

$$E_{mc} = E + RT\ln \mathrm{P_c}(E,T), \quad (2)$$

where E is the potential energy, and the second term corresponds to the bias potential. R is the gas constant, and $\mathrm{P_c}(E, T)$ denotes the canonical distribution at the temperature T:

$$\mathrm{P_c}(E,T) = \frac{\mathrm{n}(E)\exp\left(-\frac{E}{RT}\right)}{\mathrm{Z_c}(T)}, \quad (3)$$

where $\mathrm{n}(E)$ denotes the density of states, and $\mathrm{Z_c}(T)$ is the partition function of the canonical distribution at the temperature T. With this definition, the potential energy distribution of an ensemble obtained from the McMD, or the multicanonical distribution, $\mathrm{P_{mc}}(E)$, becomes uniform:

$$\mathrm{P_{mc}}(E) = \frac{\mathrm{n}(E)\exp\left(-\frac{E_{mc}}{RT}\right)}{\mathrm{Z_{mc}}(T)} = \frac{\mathrm{n}(E)\exp\left(-\frac{E}{RT}\right)}{\mathrm{P_c}(E,T)\,\mathrm{Z_{mc}}(T)} = \frac{Z_c(T)}{Z_{mc}(T)} = const. \quad (4)$$

As a result, the McMD method performs a random walk in the potential energy space and generates a uniform distribution of potential energy in a resultant ensemble. After a multicanonical ensemble is obtained, a canonical ensemble at any temperature in a sampled energy range can be generated by reweighting the probability of existence of each snapshot. Eqs. (3) and (4) include an analytical form of $\mathrm{n}(E)$, which is usually unknown *a priori*. Therefore, $\mathrm{n}(E)$ is approximated as a parametric function, e.g., the polynomial function, and its parameters are estimated by iterations of McMD simulations to make $\mathrm{P_{mc}}(E)$ near-uniform. In the i^{th} iteration, the bias potential is calculated using Eq. (2) with the canonical distribution obtained from the $(i–1)^{\mathrm{th}}$ iteration, i.e., $\mathrm{P}_{\mathrm{c}}^{i-1}(E,T)$. As the result of the i^{th} iteration, we obtain $\mathrm{P}_{\mathrm{mc}}^{i}(E)$. $\mathrm{P}_{\mathrm{c}}^{i}(E,T)$ can be calculated as

$$\mathrm{P}_{\mathrm{c}}^{i}(E,T) = \mathrm{P}_{\mathrm{mc}}^{i}(E)\mathrm{P}_{\mathrm{c}}^{i-1}(E,T). \quad (5)$$

See Ref. (Higo et al., 2012) for details.

V-McMD

V-McMD introduces a virtual system, which interacts with the molecular system, and the multicanonical ensemble is calculated for the entire system consisting of these two subsystems. (Higo, Umezawa & Nakamura, 2013) In practice, this method can be roughly interpreted as a combination of McMD and the simulated tempering method. The simulated tempering method replaces the system temperature with the Metropolis criterion and performs a canonical simulation until the next replacement trial. On the other hand, in V-McMD, the potential energy space is split into several regions (Figure S1), and the molecular system is trapped in one of these regions. With a certain time interval (t_{VST}), the molecular system replaces the region to be trapped. The state variable governing which region traps the molecular system is called the "virtual state," and the system defined by the virtual state is called the "virtual system." The energy range of each virtual state is defined to be overlapped with the adjacent virtual states.

When the molecular system has the potential energy E_k in the overlapped region of the i^{th} and $(i+1)^{th}$ virtual states, the state transition between these two virtual states can occur. Because this transition does not change the atomic coordinates or potential energy, the Metropolis criterion of this state transition is always satisfied. The time interval of virtual-state transitions (t_{VST}) should be determined arbitrarily by users. See Ref. (Higo, Umezawa & Nakamura, 2013) for details.

TTP

According to the theory of TTP, trajectories of multiple independent McMD runs with the same molecular system and different initial conditions can be treated as a single trajectory of an McMD simulation by concatenating the trajectories in an arbitrary order. This theory requires the condition that the initial coordinates of each run are sampled from the multicanonical distribution. Because the initial coordinates of production runs can be obtained from the near-uniform potential energy distribution generated by iterative simulations, it is expected that this condition holds. The McMD method with the TTP theory, which is called the TTP-McMD method, can be considered as a hybrid Monte Carlo sampler, by assuming that the system transitions from the last snapshot of the i^{th} run (the microscopic state m_{il}) to the first snapshot of the j^{th} run (the microscopic state m_{jf}) via a Monte Carlo step (Figure S2). See Ref. (Ikebe et al., 2010) for details.

Simulation protocol

We studied the three molecular systems, which are Trp-cage, PGA8, and PGA20 in an explicitly solvated cubic periodic boundary cell, by using the TTP-V-McMD method. Random coil structures of Trp-cage, PGA8, and PGA20 were constructed using the Modeller software (Webb & Sali, 2016) without any template. The termini of the PGAs were capped with acetyl and N-methyl groups, and the termini of the Trp-cage were not capped. Each of these molecular models was plased into a cubic box filled by water molecules; the number of water molecules were 5,097, 2,879, and 3,800 for Trp-cage, PGA8, and PGA20, respectively. In addition, a Cl^- ion was added to the Trp-cage model to cancel the net charge of the system. The net charge of the PGA models was zero because all the Glu residues were protonated.

The system was relaxed by using the GROMACS software. (Pronk et al., 2013) Energy minimizations were successively applied using the steepest descent and conjugate gradient methods. Then, an MD simulation under a constant-pressure ensemble with the Berendsen barostat was performed for 1 ns. In the first half of the simulation, gradual heating from 10 to 300 K was applied. In the simulation, the positions of the heavy atoms of the Trp-cage were restrained, the bond lengths were not constrained, and the integration time step (Δt) was 0.5 fs. Subsequently, an additional constant-pressure relaxation was applied for 1 ns with Δt = 2.0 fs, and the covalent bonds to hydrogen atoms were constrained using the LINCS method. (Hess et al., 1997; Hess, 2008) The final configuration of each model was used for the TTP-V-McMD simulations. The cell dimensions of these configurations were 54.0378 Å, 44.6116 Å, and 49.1174 Å for Trp-cage, PGA8, and PGA20, respectively.

For each model, the following steps were performed using our MD simulation program, which is called myPresto/omegagene and is tailored for GE simulations. (Kasahara et al., 2016) The protein conformation was randomized with a constant-temperature simulation at 800 K. By using 30 snapshots taken from a trajectory with an interval of 300 ps, 30 independent runs were simulated with a gradual decrease in the temperature from 629 to 296 K to estimate the density of states. Successively, the TTP-V-McMD simulations were iteratively performed while updating the estimation of the density of states. (Higo, Umezawa & Nakamura, 2013) A total of 84 production runs were performed (N_{run} = 84) for each of three different interval times for the virtual-state transitions (t_{VST}) meaning the interval times for bias-potential replacement: t_{VST} = 0.002 ps ns, t_{VST} = 0.2 ps, and t_{VST} = 20 ps. The simulation length of each run (t_{run}) was 50 ns except for the Trp-cage model with t_{VST} = 0.2 ps, t_{run}, of which the simulation length was 200 ns. In total, 50.4 μs of trajectories were simulated as production runs. The virtual system was divided into seven states that cover the energy range corresponding to the canonical distribution from 296 to 629 K (Table S1). The velocity scaling method (Berendsen et al., 1984) was applied to maintain the system temperature.

For the potential parameters, the AMBER ff99SB-ILDN force field, (Lindorff-Larsen et al., 2010) the ion parameter presented by Joung and Cheatham, (Joung & Cheatham, 2008) and the TIP3P water model (Jorgensen et al., 1983) were applied. The electrostatic potential was calculated using the zero-multipole summation method, which is a non-Ewald scheme. (Fukuda, 2013; Fukuda, Kamiya & Nakamura, 2014) The zero-dipole condition with the damping factor α = 0 was used. (Fukuda, Yonezawa & Nakamura, 2011; Fukuda et al., 2012)

Comparison of simulated ensembles among different settings

On the basis of the trajectories obtained from of the TTP-V-McMD production runs, the effects of the simulation conditions, i.e., the time interval for bias-strength replacement (t_{VST}), the number of independent runs (N_{run}), and the simulation time of each run (t_{run}), were assessed. For the Trp-cage model, we analyzed the FEL for various conformational ensembles on the basis of the two structural parameters: the root-mean-square deviation (RMSD) of Cα atoms from the native conformation (PDB ID: 1L2Y, model 1), which is denoted as $RMSD_{native}$, and the radius of gyration (R_g). The FEL is visualized as the map of the potential of mean forces (PMF) on the plane defined by these two parameters. We defined the *reference* ensemble as the ensemble calculated for the conditions of t_{run} = 200 ns, N_{run} = 84, and t_{VST} = 0.2 ps, because it is expected to have the highest reliability owing to its abundance of samples (it comprises a total of 16.8 μs of simulations). The FELs analyzed in various conditions were compared with the reference FEL with regard to the Pearson correlation coefficient of the PMF (PCC_{PMF}). To calculate the PCC_{PMF} for a pair of FELs, bins without samples in one of the two FELs were ignored. In addition, the probability of the existence of the native conformations in each ensemble (P_{native}) was measured to characterize each ensemble. The native conformations are defined as the conformations with $RMSD_{native} \leq 2.0$ Å.

For the PGA models, the FELs were analyzed using principal component analysis (PCA) based on the Cα–Cα distances (28 and 190 dimensions for PGA8 and PGA20, respectively). The PCAs were performed using aggregations of trajectories with all the three t_{VST} conditions for each model. For each t_{VST} condition, the ensemble calculated from the entire trajectory (t_{run} = 50 ns and N_{run} = 84) was considered as the reference ensemble. The FELs were compared with regard to PCC_{PMF}, similar to the Trp-cage case.

To assess the effects of N_{run} and t_{run}, PCC_{PMF} (and P_{native} for the Trp-cage model) were calculated for ensembles with subsets of the reference trajectories. Because there are many possibilities to pick N_{run} runs from 84 runs and t_{run}-length trajectories from the entire set of trajectories, we analyzed them by using the bootstrap approach. We constructed an ensemble by taking a random sampling of N_{run} runs from 84 runs with replacement and repeated it 100 times. The statistics over the 100 ensembles were analyzed via simulation with this N_{run} setting. This process was repeatedly performed for N_{run} = 1, 2, ..., 84. For the case of t_{run}, the trajectories were split into 5-ns bins, and an ensemble was constructed by taking a random sampling of t_{run}/5 bins with replacement. We confirmed that the results of the bootstrap analyses with 100 and 200 samples were consistent (Figure S3).

The sampling efficiency was measured in terms of the frequency of traversals between low- and high-energy regions, which were defined as the ranges [E_{min}, E_{low}] and [E_{high}, E_{max}], respectively. Here, E_{min} and E_{max} denote the minimum and maximum potential energies in all the trajectories, respectively, and E_{low} and E_{high} are defined as follows.

$$E_{low} = E_{min} + X(E_{max} - E_{min}) \quad (6)$$

$$E_{high} = E_{max} - X(E_{max} - E_{min}) \quad (7)$$

X is an arbitrary parameter in the range of 0 to 0.5. We assessed X = 0.2 and 0.3. The traversal frequency $F_{travers}^{E}$ was calculated as the number of traversals between the two energy regions during 1.0 ns. The traversal frequencies of $RMSD_{native}$ and R_g ($F_{travers}^{RMSD}$ and $F_{travers}^{Rg}$, respectively) were also analyzed.

Results

In the first part of this section, the results of the Trp-cage model are described. The reference ensemble is characterized in the subsection, “FEL of folding–unfolding equilibrium of Trp-cage”. Next, the effects of the parameters t_{run}, N_{run}, and their balances are discussed in the successive subsections: “Effects of simulation time for each run,” “Effects of number of independent runs,” and “Balance between simulation time and number of runs,” respectively. Subsequently, the effects of the other parameter t_{VST} are discussed in the subsection, “Effects of frequency of bias-strength replacement.” Additionally, the following subsection, “Effects of system complexity” describes the results of the PGA8 and PGA20 models and compares them with those of the Trp-cage model.

FEL of folding–unfolding equilibrium of Trp-cage

For the Trp-cage model, we performed 34 iterations of TTP-V-McMD simulations while updating the estimation of the density of states, n(E), and obtained a near-uniform energy distribution (Figure S4). On the basis of this estimation, we performed production runs with N_{run} = 84, t_{run} = 200 ns, and t_{VST} = 0.2 ps. This is called the reference setting hereinafter. The resultant canonical ensemble reweighted at 300 K is referred to as the reference ensemble.

The FEL of the reference ensemble projected on the $RMSD_{native}$–R_g plane is shown in Figure 1A. The most stable basin corresponds to the native structure consisting of an α-helix at the N-terminus, a 3_{10}-helix at the middle, and a loop region at the C-terminus (the secondary structural elements were recognized by using the DSSP software) (Kabsch & Sander, 1983). For example, the $RMSD_{native}$ of one of the most probable structures in this basin was 0.994 Å (Figure 1B). The energy barrier (approximately 3.3 kcal/mol) was observed at $RMSD_{native} \approx 3$ Å in a low-R_g regime. Around this barrier, the 3_{10}-helix at the middle of the peptide chain was partially deformed; this deformation can be the first step of an unfolding process (Figure 1C). The details of the unfolding pathway are not discussed in this paper. The second basin was widely spread around $RMSD_{native}$ = 4–7 Å and R_g = 7–9 Å. This corresponds to the unfolded state, and examples of the unfolded structures taken from this basin are shown in Figures 1E and F. The difference in the PMF between the bottoms of the first and second stable basins was 1.014 kcal/mol, and the population of the native conformations (P_{native}) was 22.37%. The landscape is qualitatively similar to that calculated using the REMD method reported by another group (Day, Paschek & Garcia, 2010). Our TTP-V-McMD simulation successfully identified the native structure as the most stable basin in the energy landscape, by using the reference setting.

Effects of simulation time for each run

The FELs of the Trp-cage model were drawn for a variety of t_{run} values under the condition of N_{run} = 84 and compared with the reference FEL. The FELs based on the trajectories of 0–25, 0–50, and 0–100 ns are shown in Figures 2A, B, and C, respectively. The overall geometries of these FELs were qualitatively similar to the reference (Figure 1A); their PCC_{PMF} values were 0.936, 0.936, and 0.994, respectively. The bootstrap statistics of PCC_{PMF} for each t_{run} value are summarized in Figure 2D. For t_{run} = 200 ns, the bootstrap average and the standard deviation (SD) of PCC_{PMF} were 0.990 and 0.00720, respectively. Even in the worst case among 100 randomly generated ensembles with t_{run} = 200 ns, PCC_{PMF} was 0.966. From this condition, a decrease in t_{run} yielded a slow decay of PCC_{PMF}, and PCC_{PMF} reached 0.9 at $t_{run} \approx 30$ ns, which corresponds to 15% of the samples in the reference. Further decreasing t_{run} resulted in a steep decrease of PCC_{PMF}. Along with the decrease of the bootstrap average of PCC_{PMF}, the SD was increased. This means that an insufficient simulation time causes a loss of robustness of the results.

In contrast to the fact that the PCC_{PMF} decays in a shorter t_{run} than the reference, the balance between the folded and unfolded states (P_{native}) was almost constant regardless of t_{run} (Figure 2E); the bootstrap average of P_{native} for t_{run} = 5–200 ns was in the range of 0.220 to 0.225. However, the SD of P_{native} was reduced with the increase of t_{run}; the SDs of P_{native} at t_{run} = 5, 50,

and 200 ns were 0.0658, 0.0198, and 0.00838, respectively. The loss of robustness due to the insufficiency of the simulation time is demonstrated in terms of not only the similarity of the entire FEL but also the stability of the native fold.

Effects of number of independent runs

As in the previous subsection, the effects of the reduction of N_{run} on the FELs were assessed under the condition of t_{run} = 200 ns. Examples of FELs with N_{run} = 10, 21, and 42 are shown in Figures 3A, B, and C, respectively; the PCC_{PMF} values were 0.637, 0.939, and 0.993, respectively. Although the positions and wideness of the basins were similar to the reference, the FELs with a smaller N_{run} were smoother and lacked small bumps on the landscapes. The bootstrap statistics of PCC_{PMF} for various N_{run} values (Figure 3D) were similar to those for t_{run} (Figure 2D). The quantity of the samples required for $PCC_{PMF} \geq 0.9$ was approximately one-fourth of the reference ($N_{run} \approx 21$). The average (and the SD) of PCC_{PMF} at N_{run} = 21 and 42 were 0.906 (0.0733) and 0.956 (0.0399), respectively. Larger N_{run} values are needed to obtain robust results.

Regarding P_{native}, the influence of the reduction of N_{run} (Figure 3E) differed from that of the reduction of t_{run} (Figure 2E). A lower N_{run} resulted in the underestimation of the population of native conformations. P_{native} reached at plateau for $N_{run} \geq 21$. A certain number of runs was needed to obtain robust results, and t_{run} = 200 ns was too short to reach equilibrium with a small number of trajectories for this system.

Balance between simulation time and number of runs

The evaluation for various t_{run} values with N_{run} = 84 runs (Figure 2) and that for various N_{run} values with t_{run} = 200 ns (Figure 3) indicate that reducing t_{run} produced better results than reducing N_{run} if the cumulative simulation time ($N_{run} \times t_{run}$) was the same. Figure 4 shows direct comparisons of the results, indicating that high-N_{run} conditions resulted in a higher PCC_{PMF} and more similar values of P_{native} to the reference, with lower SDs, than long-t_{run} conditions. In particular, the qualitative difference between the two strategies is shown by the mean of P_{native}. Reducing N_{run} resulted in the significant underestimation of the fold stability, but reducing t_{run} did not.

In addition, we performed bootstrap analyses for all the combinations of 40-t_{run} settings (5, 10, 15, ..., 200 ns) and 21-N_{run} settings (4, 8, 12, ..., 84). The average values of PCC_{PMF} and P_{native} in all the conditions are presented in Figures 5 and S5. The PCC_{PMF} was proportional to $\log(N_{run} \times t_{run})$. While the trend of P_{native} is ambiguous, the use of a larger number of samples resulted in a higher P_{native}. In the case where only small amount of data was available, a lower ratio of t_{run}/N_{run} (purple plots in Figure 5) yielded better results.

Effects of frequency of bias-strength replacement

The parameter t_{VST} controls the frequency of the bias-strength switching in the TTP-V-McMD method. We investigated the effects of this parameter by comparing the TTP-V-McMD

simulations of the Trp-cage model under the three conditions—t_{VST} = 0.002, 0.2, and 20 ps—with t_{run} = 50 ns for N_{run} = 84.

Table 1 summarizes the frequency of traversals between high- and low-potential energy regimes (F_{trv}^{E}), as defined in Eqs. (6) and (7) with X = 0.3 and 0.2, as well as the frequency of traversals between $RMSD_{native}$ (F_{trv}^{RMSD}) and R_g (F_{trv}^{Rg}). The simulations with a shorter t_{VST} resulted in faster traversals in the potential energy space, indicating that with a shorter t_{VST}, a wider potential energy range can be sampled in a shorter time. However, faster traversal in the potential energy space does not ensure faster transition of the protein conformation. For both X = 0.2 and 0.3, although the setting of t_{VST} = 0.002 ps yielded the highest F_{trv}^{E}, this condition did not yield a higher F_{trv}^{RMSD} and F_{trv}^{Rg} compared to when a longer t_{VST} was used. This result indicates that the relaxation of the conformation requires a longer time than that of the potential energy. If a strong bias is applied and the system takes a high-potential energy state, it can return to low-energy states before conformational changes. Therefore, a moderate speed for traversals in the potential energy space is ideal for efficient conformational sampling. In the case of X = 0.2, t_{VST} = 0.2 ps exhibited the most frequent conformational changes.

In addition, the resultant ensembles were slightly affected by the setting of t_{VST}. We analyzed P_{native} for ensembles of various t_{run} values with N_{run} = 84 using the bootstrap method (Figure S6). The results for all three t_{VST} values showed similar trends, i.e., near-constant average values and the gradual decay of the SD with the increase of t_{run}. While t_{VST} = 0.2 ps showed a smaller P_{native} than the other two t_{VST} settings, the difference was smaller than the SD. On the other hand, higher SD values were observed in the following order: t_{VST} = 0.2 > 20 > 0.002 ps. This is consistent with the order of F_{trv}^{RMSD} and F_{trv}^{Rg} (Table 1). The result indicates that more frequent traversals between high- and low-$RMSD_{native}$ conformations make it possible to explore a wider region of the conformational space; thus, the population of the native conformation decreases, and the SD increases.

Regarding the PCC_{PMF} with the reference setting (t_{VST} = 0.2 ps, N_{run} = 84, and t_{run} = 200 ns), the average PCC_{PMF} values at t_{run} = 50 ns differed among different settings of t_{VST} (Figure S6). This indicates that changing t_{VST} yields subtle differences in the resultant ensemble. Regarding the balance between t_{run} and N_{run}, the trends were similar for all the settings of t_{VST} (Figure S7).

Effects of system complexity: comparison with the PGA models

We performed the same analyses for the molecular models of PGA8 and PGA20. In contrast to Trp-cage, these peptides did not exhibit a particular fold. The FELs of both PGA8 and PGA20 were unimodal distributions, the basins of which consisted of a variety of collapsed conformations (Figure 6 for t_{VST} = 0.2 ps). The ensembles included short secondary structural elements but they were unstable. Although the shape of the small bumps in the basins differred depending on the simulation conditions, the overall geometries of the FELs were similar (Figure S8 for t_{VST} = 0.002 ps and 20 ps).

Regarding the balance between t_{run} and N_{run}, Figure 7 shows the bootstrap averages of PCC_{PMF} between the ensemble calculated by the full-length trajectory (t_{run} = 50 ns and N_{run} = 84) and those calculated by the reduced trajectories. No clear differences were found between the PCC_{PMF} curve with reduced t_{run} and that with reduced N_{run} for both the PGA8 and PGA20 (Figure 7 for t_{VST} = 0.2 ps; Figure S9 for the other conditions). A small number of long simulations exhibited the similar efficiency as that of many short simulations. In addition, no significant differences were found between the results of PGA8 and PGA20. It is noteworthy that the conformational space of PGA20 is considerably wider than that of PGA8 and similar to that of Trp-cage, because the conformational space volume of polypeptides is determined primarily by their length, Therefore, we concluded that the effects of balance between t_{run} and N_{run} are determined by the complexity of the FEL (e.g., existence of the free-energy barrier) rather than the conformational space volume. An increase in the number of runs is more effective for a system with more complex FEL.

For the PGA models, the frequencies of traversals in the potential energy and R_g spaces (F_{trv}^{E} and F_{trv}^{Rg}, respectively) are summarized in Table 2. Both the PGA8 and PGA20 models yielded similar trends as the Trp-cage model (Table 1). Although frequent replacements of bias-potential strength enhanced the traversals in the potential energy space, they did not enhance the conformational changes in terms of R_g. This implies that the conformational changes are much slower than the potential energy changes even if there is no free-energy barrier exists in the landscape. However, in contrast to the Trp-cage case, the drawback of the frequent replacement, that is, slow traversals in the conformational space, is unclear in the case of PGA20.

Discussion

We examined the performance of the TTP-V-McMD method with regard to two adjustable settings: (i) the balance between the number of runs (N_{run}) and the simulation length in each run (t_{run}) and (ii) the frequency of the bias-strength switching (t_{VST}). For (i), in the Trp-cage model including folding–unfolding transition, we found higher robustness of the conditions with a larger number of runs than with longer simulations. In particular, the probability of the existence of native conformations in a resultant ensemble (P_{native}) was more sensitive to the condition than the entire similarity of the FEL. However, for the cases of PGAs without free-energy barrier in their FELs, no significant effect was shown in the balance between the number and length of simulations. Therefore, the optimal balance depended on the molecular system, and the complexity of the FELs was a key feature rather than the degree of freedom. In any case, increasing the number of simulations was recommended because it is not worse than increasing the length of each run. This result is practically useful because performing many parallel runs is easier than executing a single long simulation. While the result obtained here encourages performing many short runs, it requires the condition that the initial structures of the production runs are uniformly sampled from the multicanonical ensemble, whose energy distribution is uniform. (Ikebe et al., 2010) As our protocol samples the initial structures of the production runs from the previous iteration of the McMD, it is expected that this condition holds.

For (ii), whereas higher frequencies of bias-strength replacement enhance the sampling of a wider range of potential energy, they do not ensure the enhancement of the sampling of a wider range of conformations. This means that the enhancement of the sampling along one variable (e.g., potential energy or temperature) does not ensure the enhancement of the sampling along another variable (e.g., RMSD and R_g). Rapid traversals in the energy space sometimes obtain a high energy and return to the low-energy regime before conformational change regardless of the existence of free-energy barrier in the FEL. A moderate frequency is needed to maximize the performance for any molecular system.

The findings that we obtained by applying the TTP-V-McMD method provide insight into the characteristics of many other GE methods. (i) For GE methods that involve running independent parallel simulations, e.g., simulated tempering and AUS, performing many short runs can be more effective than increasing the length of each run. For GE methods where parallel runs are coupled, e.g., the REMD method, this conclusion should not be simply applied. For example, an increase in the number of runs in the REMD method resulted in larger overlaps of the distributions of neighboring replicas, along with an increase in the acceptance probability of replica-exchange trials. Our previous evaluation for the REMD method showed that a larger number of replicas does not always yield better results. (Iwai, Kasahara & Takahashi, 2018) The number of runs should be adjusted independently from the coupling condition of the parallel runs; for example, the number of runs in a REMD simulation could be increased by performing two or more independent REMD simulations with different initial conformations, and aggregating the resultant ensembles. (ii) Regarding the frequency of the bias-strength replacement, the conclusion that the interval should be long enough to relax the conformation could be transferred to other GE methods. For the REMD methods, the effects of the interval for replica-exchange trials have been reported; while some studies recommended shorter intervals (Sindhikara, Meng & Roitberg, 2008; Sindhikara, Emerson & Roitberg, 2010), the side effects of highly frequent exchange trials have also been reported and were consistent to our result (Periole & Mark, 2007; Iwai, Kasahara & Takahashi, 2018).

Conclusions

In this study, the effects of two parameters of GE methods, i.e., (i) the balance between the number of runs (N_{run}) and the simulation length in each run (t_{run}) and (ii) the frequency of the bias-strength switching (t_{VST}) were extensively examined with using all-atom explicit-solvent models of three polypeptides that are a foldable mini-protein and disordered peptides. We suggest a guide to adjust the setting for general molecular systems and GE methods. (i) Increasing in the number of runs should be prioritized rather than increasing the simulation length. (ii) Highly frequent replacements of the bias potentials may yield side effects because conformational relaxation was slower than potential energy relaxation. The time interval for replacement should be longer than or equal to 0.2 ps.

Acknowledgements

The MD simulations were performed using the TSUBAME3 supercomputer at the Tokyo Institute of Technology, provided through the HPCI System Research Projects (Project IDs: hp180050, hp180054, hp190017, and hp190018). The numerical computations for post-simulation analyses were performed using the supercomputer system provided by the National Institute of Genetics, Research Organization of Information and Systems, Japan.

References

Abraham MJ, Murtola T, Schulz R, Páll S, Smith JC, Hess B, Lindahl E 2015. GROMACS: High performance molecular simulations through multi-level parallelism from laptops to supercomputers. *SoftwareX* 1-2:19–25.

Ahmed Z, Beta IA, Mikhonin AV, Asher SA 2005. UV−Resonance Raman Thermal Unfolding Study of Trp-Cage Shows That It Is Not a Simple Two-State Miniprotein. *Journal of the American Chemical Society* 127:10943–10950. DOI: 10.1021/ja050664e.

Berendsen HJC, Postma JPM, van Gunsteren WF, DiNola A, Haak JR 1984. Molecular dynamics with coupling to an external bath. *Journal of Chemical Physics* 81:3684–3690. DOI: 10.1063/1.448118.

Clarke DT, Doig AJ, Stapley BJ, Jones GR 1999. The alpha-helix folds on the millisecond time scale. *Proceedings of the National Academy of Sciences of the United States of America* 96:7232–7237. DOI: 10.1073/pnas.96.13.7232.

Day R, Paschek D, Garcia AE 2010. Microsecond simulations of the folding/unfolding thermodynamics of the Trp-cage miniprotein. *Proteins: Structure, Function, and Bioinformatics* 78:1889–1899. DOI: 10.1002/prot.22702.

Donten ML, Hamm P 2013. pH-jump induced α-helix folding of poly-l-glutamic acid. *Chemical Physics* 422:124–130. DOI: 10.1016/j.chemphys.2012.11.023.

Finke JM, Jennings PA, Lee JC, Onuchic JN, Winkler JR 2007. Equilibrium unfolding of the poly(glutamic acid)20 helix. *Biopolymers* 86:193–211. DOI: 10.1002/bip.20719.

Fukuda I 2013. Zero-multipole summation method for efficiently estimating electrostatic interactions in molecular system. *The Journal of chemical physics* 139:174107. DOI: 10.1063/1.4827055.

Fukuda I, Kamiya N, Nakamura H 2014. The zero-multipole summation method for estimating electrostatic interactions in molecular dynamics: Analysis of the accuracy and application to liquid systems. *The Journal of chemical physics* 140:194307. DOI: 10.1063/1.4875693.

Fukuda I, Kamiya N, Yonezawa Y, Nakamura H 2012. Simple and accurate scheme to compute electrostatic interaction: Zero-dipole summation technique for molecular system and application to bulk water. *The Journal of Chemical Physics* 137:054314. DOI: 10.1063/1.4739789.

Fukuda I, Yonezawa Y, Nakamura H 2011. Molecular dynamics scheme for precise estimation of electrostatic interaction via zero-dipole summation principle. *The Journal of Chemical Physics* 134:164107. DOI: 10.1063/1.3582791.

Hałabis A, Żmudzińska W, Liwo A, Ołdziej S 2012. Conformational Dynamics of the Trp-Cage Miniprotein at Its Folding Temperature. *The Journal of Physical Chemistry B* 116:6898–6907. DOI: 10.1021/jp212630y.

Hess B 2008. P-LINCS: A Parallel Linear Constraint Solver for Molecular Simulation. *Journal*

of Chemical Theory and Computation 4:116–122. DOI: 10.1021/ct700200b.

Hess B, Bekker H, Berendsen HJC, Fraaije JGEM 1997. LINCS: a linear constraint solver for molecular simulations. *Journal of computational chemistry* 18:1463–1472.

Higo J, Dasgupta B, Mashimo T, Kasahara K, Fukunishi Y, Nakamura H 2015. Virtual-system-coupled adaptive umbrella sampling to compute free-energy landscape for flexible molecular docking. *Journal of computational chemistry* 36:1489–1501. DOI: 10.1002/jcc.23948.

Higo J, Ikebe J, Kamiya N, Nakamura H 2012. Enhanced and effective conformational sampling of protein molecular systems for their free energy landscapes. *Biophysical Reviews* 4:27–44. DOI: 10.1007/s12551-011-0063-6.

Higo J, Umezawa K, Nakamura H 2013. A virtual-system coupled multicanonical molecular dynamics simulation: Principles and applications to free-energy landscape of protein–protein interaction with an all-atom model in explicit solvent. *The Journal of Chemical Physics* 138:184106. DOI: 10.1063/1.4803468.

Ikebe J, Umezawa K, Kamiya N, Sugihara T, Yonezawa Y, Takano Y, Nakamura H, Higo J 2010. Theory for trivial trajectory parallelization of multicanonical molecular dynamics and application to a polypeptide in water. *Journal of computational chemistry* 32:1286–1297. DOI: 10.1002/jcc.21710.

Iwai R, Kasahara K, Takahashi T 2018. Influence of various parameters in the replica-exchange molecular dynamics method: Number of replicas, replica-exchange frequency, and thermostat coupling time constant. *Biophysics and Physicobiology* 15:165–172. DOI: 10.2142/biophysico.15.0_165.

Jani V, Sonavane UB, Joshi R 2014. REMD and umbrella sampling simulations to probe the energy barrier of the folding pathways of engrailed homeodomain. *Journal of Molecular Modeling* 20:2283. DOI: 10.1007/s00894-014-2283-8.

Jorgensen WL, Chandrasekhar J, Madura JD, Impey RW, Klein ML 1983. Comparison of simple potential functions for simulating liquid water. *The Journal of chemical physics* 79:926–935. DOI: 10.1063/1.445869.

Joung IS, Cheatham TE 2008. Determination of Alkali and Halide Monovalent Ion Parameters for Use in Explicitly Solvated Biomolecular Simulations. *The Journal of Physical Chemistry B* 112:9020–9041. DOI: 10.1021/jp8001614.

Kabsch W, Sander C 1983. Dictionary of protein secondary structure: Pattern recognition of hydrogen-bonded and geometrical features. *Biopolymers* 22:2577–2637. DOI: 10.1002/bip.360221211.

Kasahara K, Ma B, Goto K, Dasgupta B, Higo J, Fukuda I, Mashimo T, Akiyama Y, Nakamura H 2016. myPresto/omegagene: a GPU-accelerated molecular dynamics simulator tailored for enhanced conformational sampling methods with a non-Ewald electrostatic scheme. *Biophysics and Physicobiology* 13:209–216. DOI: 10.2142/biophysico.13.0_209.

Kimura T, Takahashi S, Akiyama S, Uzawa T, Ishimori K, Morishima I 2002. Direct Observation of the Multistep Helix Formation of Poly- l-glutamic Acids. *Journal of the American Chemical Society* 124:11596–11597. DOI: 10.1021/ja026639f.

Lindorff-Larsen K, Piana S, Palmo K, Maragakis P, Klepeis JL, Dror RO, Shaw DE 2010. Improved side-chain torsion potentials for the Amber ff99SB protein force field. *Proteins: Structure, Function, and Bioinformatics* 78:1950–1958. DOI: 10.1002/prot.22711.

Nakajima N, Nakamura H, Kidera A 1997. Multicanonical Ensemble Generated by Molecular Dynamics Simulation for Enhanced Conformational Sampling of Peptides. *The Journal of Physical Chemistry B* 101:817–824. DOI: 10.1021/jp962142e.

564 Ogasawara N, Kasahara K, Iwai R, Takahashi T 2018. Unfolding of α-helical 20-residue poly-
565 glutamic acid analyzed by multiple runs of canonical molecular dynamics simulations. *PeerJ*
566 6:e4769. DOI: 10.7717/peerj.4769.
567 Periole X, Mark AE 2007. Convergence and sampling efficiency in replica exchange simulations
568 of peptide folding in explicit solvent. *Journal of Chemical Physics* 126:014903. DOI:
569 10.1063/1.2404954.
570 Péter Hudáky, Pál Stráner, Viktor Farkas, Györgyi Váradi, Gábor Tóth A, András Perczel 2007.
571 Cooperation between a Salt Bridge and the Hydrophobic Core Triggers Fold Stabilization in
572 a Trp-Cage Miniprotein†. *Biochemistry* 47:1007–1016. DOI: 10.1021/bi701371x.
573 Pronk S, Páll S, Schulz R, Larsson P, Bjelkmar P, Apostolov R, Shirts MR, Smith JC, Kasson
574 PM, van der Spoel D, Hess B, Lindahl E 2013. GROMACS 4.5: a high-throughput and
575 highly parallel open source molecular simulation toolkit. *Bioinformatics (Oxford, England)*
576 29:845–854. DOI: 10.1093/bioinformatics/btt055.
577 Rosta E, Hummer G 2009. Error and efficiency of replica exchange molecular dynamics
578 simulations. *Journal of Chemical Physics* 131:165102. DOI: 10.1063/1.3249608.
579 Salomon-Ferrer R, Götz AW, Poole D, Le Grand S, Walker RC 2013. Routine Microsecond
580 Molecular Dynamics Simulations with AMBER on GPUs. 2. Explicit Solvent Particle Mesh
581 Ewald. *Journal of Chemical Theory and Computation* 9:3878–3888. DOI:
582 10.1021/ct400314y.
583 Shaw DE, Grossman JP, Bank JA, Batson B, Butts JA, Chao JC, Deneroff MM, Dror RO, Even
584 A, Fenton CH, Forte A, Gagliardo J, Gill G, Greskamp B, Ho CR, Ierardi DJ, Iserovich L,
585 Kuskin JS, Larson RH, Layman T, Lee L-S, Lerer AK, Li C, Killebrew D, Mackenzie KM,
586 Mok SY-H, Moraes MA, Mueller R, Nociolo LJ, Peticolas JL, Quan T, Ramot D, Salmon
587 JK, Scarpazza DP, Ben Schafer U, Siddique N, Snyder CW, Spengler J, Tang PTP, Theobald
588 M, Toma H, Towles B, Vitale B, Wang SC, Young C 2014. Anton 2: raising the bar for
589 performance and programmability in a special-purpose molecular dynamics supercomputer.
590 In: IEEE Press, 41–53. DOI: 10.4324/9780203843550.
591 Shirts MR, Chodera JD 2008. Statistically optimal analysis of samples from multiple equilibrium
592 states. *The Journal of chemical physics* 129:124105. DOI: 10.1063/1.2978177.
593 Sindhikara DJ, Emerson DJ, Roitberg AE 2010. Exchange Often and Properly in Replica
594 Exchange Molecular Dynamics. *Journal of chemical theory and computation* 6:2804–2808.
595 DOI: 10.1021/ct100281c.
596 Sindhikara D, Meng Y, Roitberg AE 2008. Exchange frequency in replica exchange molecular
597 dynamics. *The Journal of chemical physics* 128:024103. DOI: 10.1063/1.2816560.
598 Souaille M, Roux B 2001. Extension to the weighted histogram analysis method: combining
599 umbrella sampling with free energy calculations. *Computer Physics Communications*
600 135:40–57.
601 Sugita Y, Okamoto Y 1999. Replica-exchange molecular dynamics method for protein folding.
602 *Chemical Physics Letters* 314:141–151.
603 Webb B, Sali A 2016. Comparative Protein Structure Modeling Using MODELLER. *Current*
604 *protocols in bioinformatics / editoral board, Andreas D. Baxevanis ... [et al.]* 54:5.6.1–
605 5.6.37. DOI: 10.1002/cpbi.3.
606

Figure 1(on next page)

FEL calculated by the reference ensemble of Trp-cage.

(A) FEL based on the $RMSD_{native}$–R_g plane. The color gradation indicates the PMF. (B) Snapshot taken from the first basin (blue) superimposed on the experimentally solved structure (gray; PDB ID: 1Y2L, model 1). (C) Examples of snapshots near the first basin. The structures colored dark cyan and light cyan correspond to the positions C1 and C2 marked in (A), respectively. (D, E) Examples of unfolded structures in the second basin. The positions of each snapshot on the FEL are marked in (A).

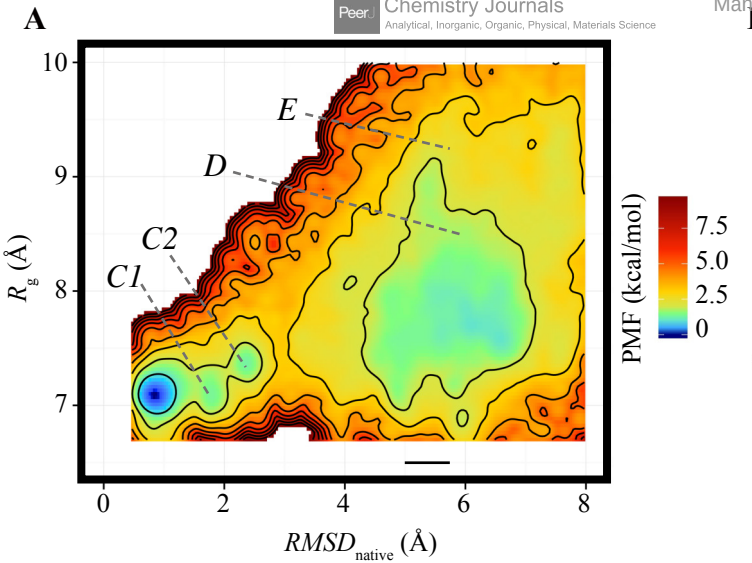
A
10
9
8
7
R_g (Å)
E
D
C2
C1
0
2
4
6
8
$RMSD_{native}$ (Å)
PMF (kcal/mol)
7.5
5.0
2.5
0

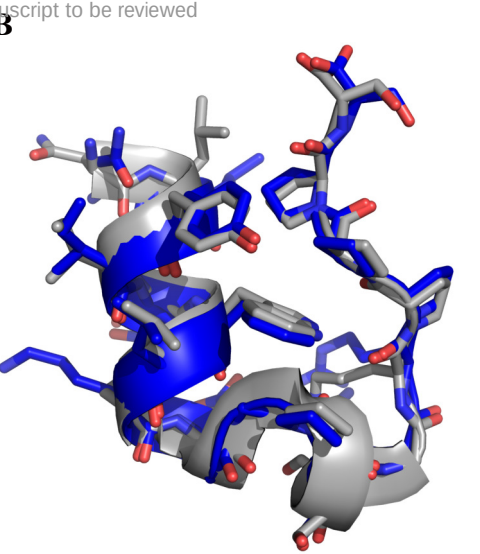
B

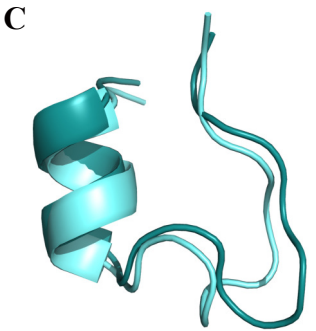
C

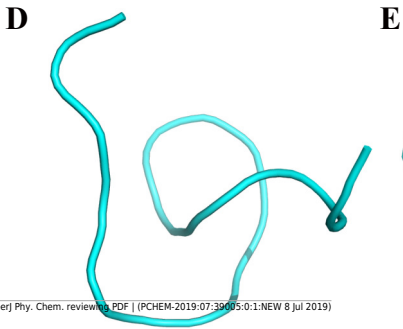
D


E

Figure 2(on next page)

FELs of Trp-cage for various t_{run} values with N_{run} = 84.

(A, B, C) FELs based on the trajectories of 0–25 ns (A), 0–50 ns (B), and 0–100 ns (C). (D) Bootstrap statistics of PCC_{PMF}. The solid line is the average, the dashed lines are the sum of the average and SD and the subtraction of the SD from average. The dotted lines indicate the maximum and minimum values among 100 randomly generated ensembles in each condition. (E) Statistics of P_{native} shown in the same scheme as (D).

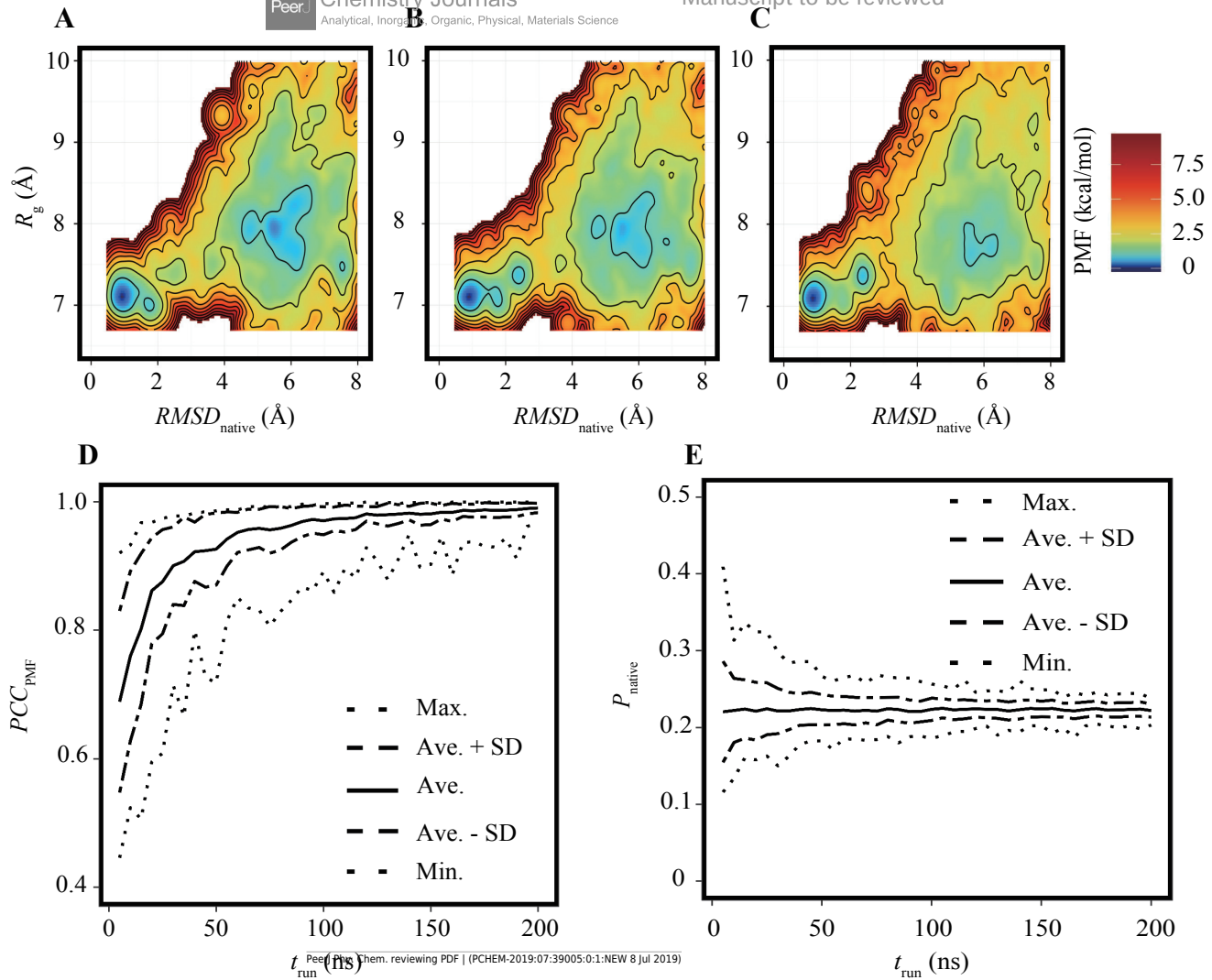
A
B
C
R_g (Å)
$RMSD_{native}$ (Å)
PMF (kcal/mol)
7.5
5.0
2.5
0
D
E
PCC_{PMF}
P_{native}
t_{run} (ns)
Max.
Ave. + SD
Ave.
Ave. - SD
Min.

Figure 3(on next page)

Characteristics of FELs of Trp-cage for smaller N_{run} values with t_{run} = 200 ns.

(A, B, C) Examples of FELs with N_{run} = 10 (A), N_{run} = 21 (B), and N_{run} = 42 (C). (D, E) Bootstrap statistics of PCC_{PMF} (D) and P_{native} (E). See also the legend of Figure 2.

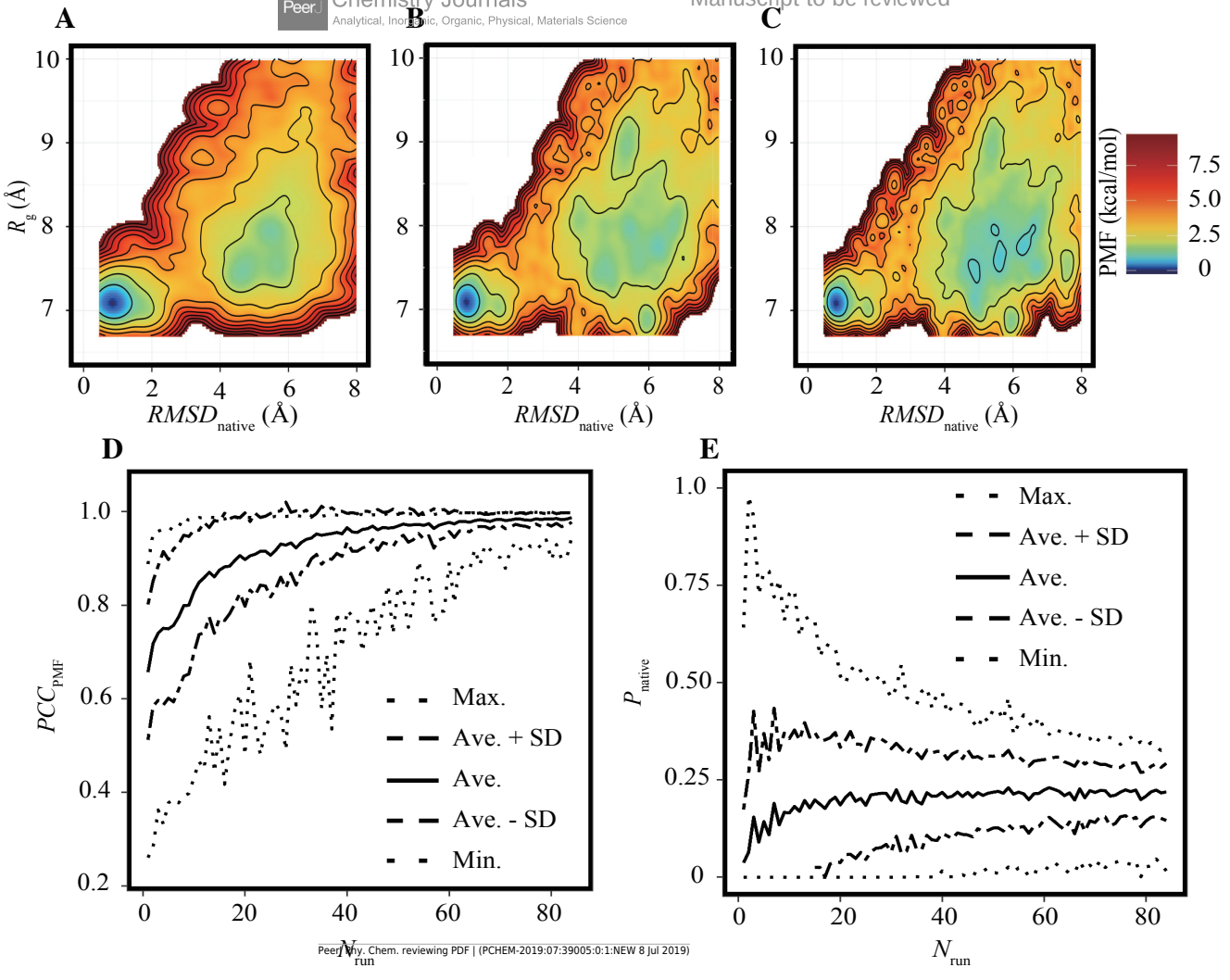
A
B
C
D
E
R_g (Å)
$RMSD_{native}$ (Å)
PMF (kcal/mol)
7.5
5.0
2.5
0
PCC_{PMF}
P_{native}
N_{run}
Max.
Ave. + SD
Ave.
Ave. - SD
Min.

Figure 4(on next page)

Direct comparison between reducing t_{run} with the fixed-N_{run} condition (blue line) and reducing N_{run} with the fixed-t_{run} condition (red line) for the Trp-cage model.

The vertical axes indicate (A) the average of PCC_{PMF}, (B) the SD of PCC_{PMF}, (C) the average of P_{native}, and (D) the SD of P_{native}. The horizontal axis indicates the accumulated simulation length ($N_{run} \times t_{run}$).

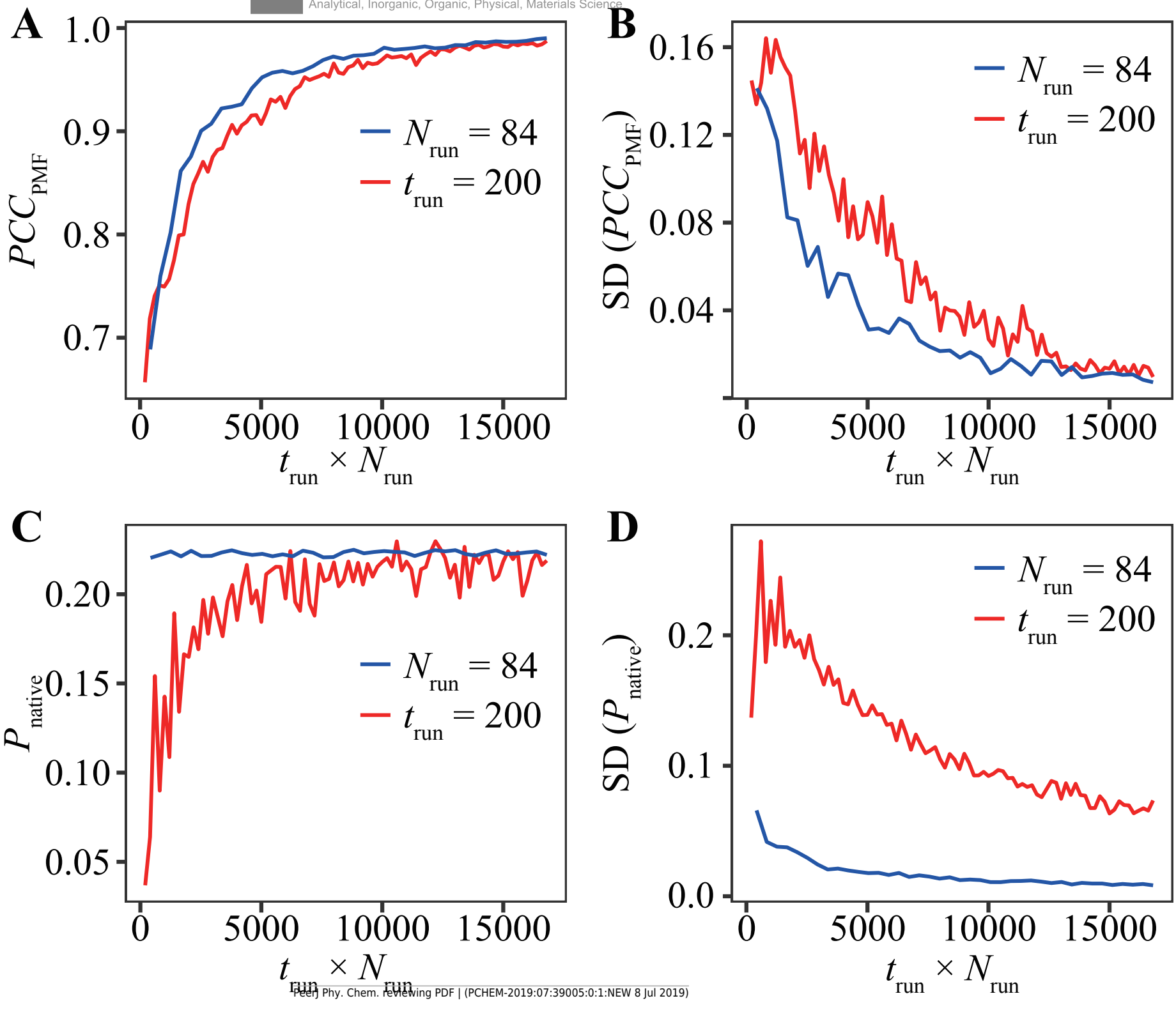
A
B
C
D
PCC_{PMF}
SD (PCC_{PMF})
P_{native}
SD (P_{native})
$N_{run} = 84$
$t_{run} = 200$
$t_{run} \times N_{run}$
0
5000
10000
15000
1.0
0.9
0.8
0.7
0.16
0.12
0.08
0.04
0.20
0.15
0.10
0.05
0.2
0.1
0.0

Figure 5(on next page)

Distribution of (A) the average of PCC_{PMF} and (B) P_{native} along the logarithm of the accumulated simulation length for various combinations of N_{run} and t_{run} extracted from the trajectories th

The color of each plot indicates the log-ratio of N_{run} to t_{run} compared with the reference. The definition is $\log[(t_{run}/N_{run})/(200/84)]$. This value becomes greater than 0 for conditions with a higher ratio of t_{run} to N_{run} than the reference.

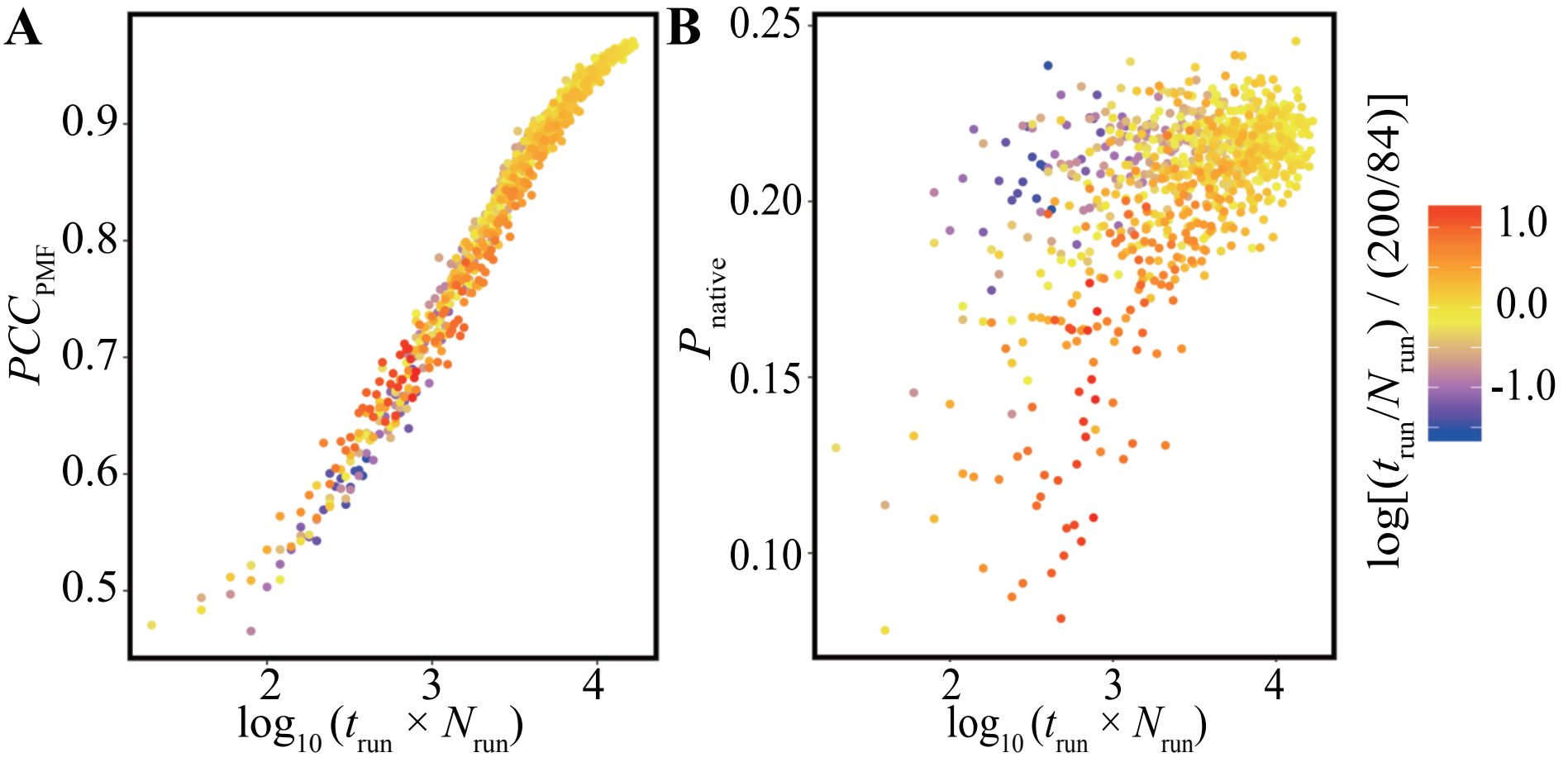
A
B
PCC_{PMF}
P_{native}
$\log_{10}(t_{run} \times N_{run})$
$\log[(t_{run}/N_{run}) / (200/84)]$
0.5
0.6
0.7
0.8
0.9
0.10
0.15
0.20
0.25
2
3
4
1.0
0.0
-1.0

Figure 6(on next page)

FELs calculated by ensembles of (A) PGA8 and (B) PGA20 using t_{run} = 50 ns and N_{run} = 84 with t_{VST} = 0.002 ps.

(C, D, E) Examples of snapshots in the basins marked in the panels (A) and (B).

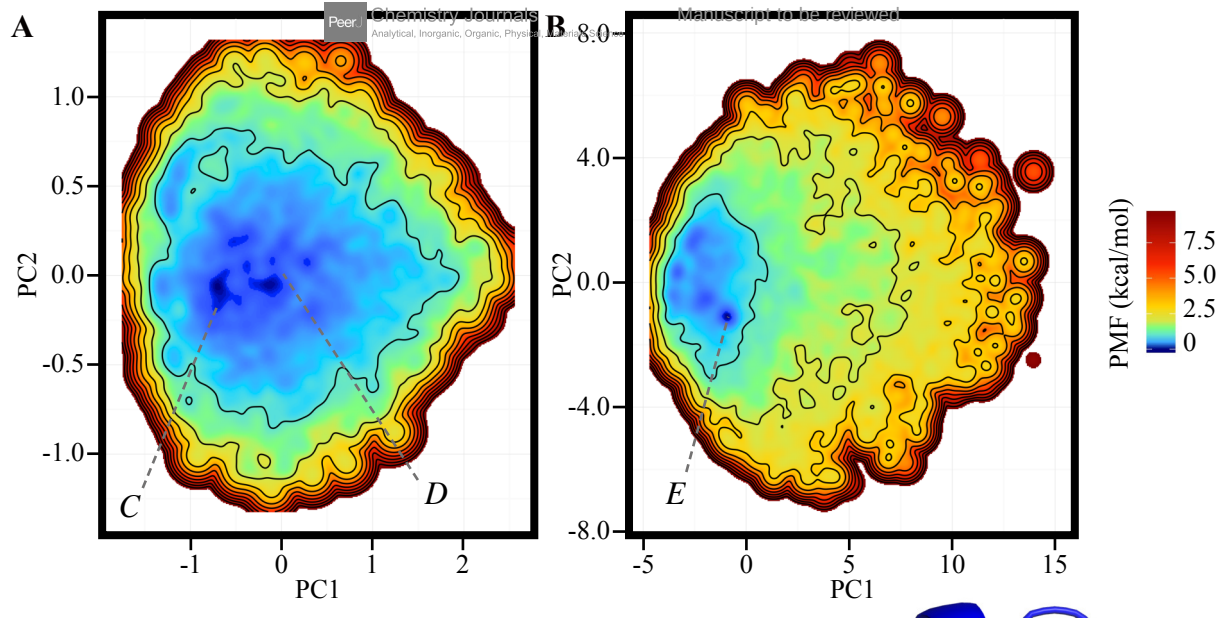

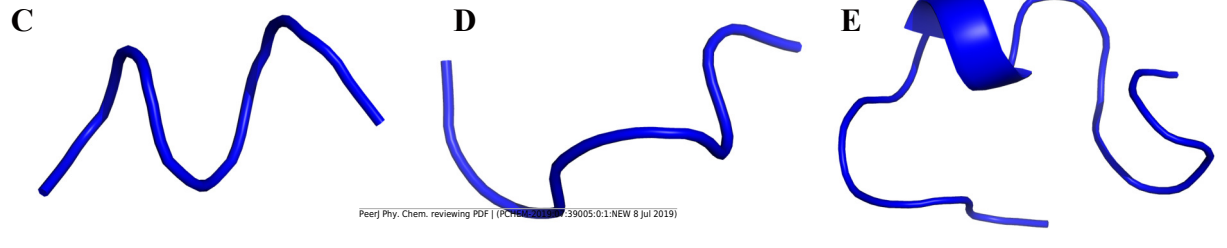

Figure 7 (on next page)

Direct comparisons between reducing t_{run} with fixed-N_{run} (blue line) and reducing N_{run} with fixed-t_{run} (red line) for (A, B) the PGA8 and (C, D) PGA20 systems.

The vertical axes indicate (A, C) the bootstrap average of PCC_{PMF}, and (B, D) the SD of PCC_{PMF}. The horizontal axis indicates the accumulated simulation length ($N_{run} \times t_{run}$). The results of t_{VST} = 0.2 ps are presented. See also Figure S9 for the other t_{VST} conditions.

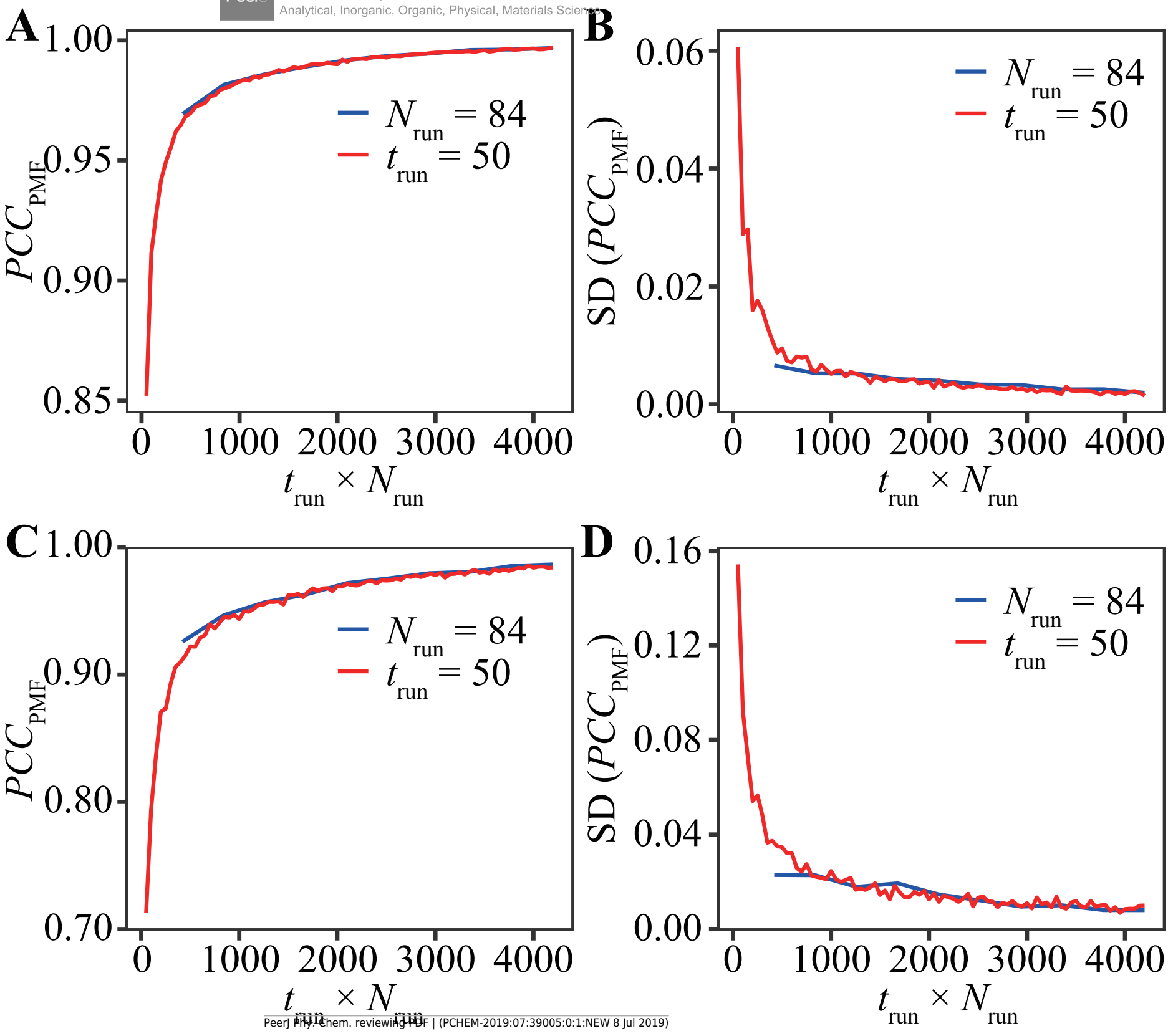
A
B
C
D
PCC_{PMF}
SD (PCC_{PMF})
$N_{run} = 84$
$t_{run} = 50$
$t_{run} \times N_{run}$
1.00
0.95
0.90
0.85
0.80
0.70
0.06
0.04
0.02
0.00
0.16
0.12
0.08
0.04
0
1000
2000
3000
4000

Table 1(on next page)

Average values (and the standard errors) of the traversal frequencies over 84 runs for the Trp-cage model.

Table 1. Average values (and the standard errors) of the traversal frequencies over 84 runs for the Trp-cage model.

t_{VST} (ps)	0.002	0.2	20
X		0.3	
F_{trv}^{E} (ns^{-1})	1.63 (0.06)	1.45 (0.04)	1.02 (0.04)
F_{trv}^{RMSD} (ns^{-1})	0.057 (0.006)	0.060 (0.004)	0.062 (0.006)
F_{trv}^{Rg} (ns^{-1})	0.040 (0.005)	0.044 (0.003)	0.050 (0.006)
X		0.2	
F_{trv}^{E} (ns^{-1})	0.70 (0.03)	0.62 (0.02)	0.46 (0.02)
F_{trv}^{RMSD} (ns^{-1})	0.005 (0.001)	0.011 (0.001)	0.006 (0.002)
F_{trv}^{Rg} (ns^{-1})	0.008 (0.002)	0.012 (0.001)	0.007 (0.002)

Table 2(on next page)

Average values (and standard errors) of the traversal frequencies over 84 runs for PGA models.

Table 2. Average values (and standard errors) of the traversal frequencies over 84 runs for PGA models.

Model	PGA8			PGA20		
t_{VST} (ps)	0.002	0.2	20	0.002	0.2	20
X	0.3			0.3		
F_{trv}^{E} (ns^{-1})	2.91 (0.03)	2.70 (0.03)	0.86 (0.02)	1.05 (0.04)	0.99 (0.03)	0.46 (0.02)
F_{trv}^{Rg} (ns^{-1})	0.44 (0.02)	0.47 (0.02)	0.47 (0.02)	0.045 (0.005)	0.044 (0.005)	0.049 (0.006)
X	0.2			0.2		
F_{trv}^{E} (ns^{-1})	1.58 (0.02)	1.53 (0.02)	0.50 (0.01)	0.4 (0.02)	0.41 (0.01)	0.22 (0.01)
F_{trv}^{Rg} (ns^{-1})	0.117 (0.007)	0.147 (0.007)	0.146 (0.007)	0.011 (0.002)	0.013 (0.002)	0.015 (0.003)